Enhancer of zeste homolog 2 facilitates phenotypic transition of vascular smooth muscle cells leading to aortic aneurysm/dissection

SHISHAN XUE[1,2*], SHUAI LENG[1*], FENGQUAN ZHANG[1*], ZHIQIAO DANG[1], GUOHAI SU[1,2] and WENQIAN YU[1]

[1]Department of Cardiac Surgery, Research Center of Translational Medicine, Jinan Central Hospital Affiliated to Shandong First Medical University, Jinan, Shandong 250013; [2]Department of Cardiovascular Medicine, Jinan Central Hospital, Shandong University, Jinan, Shandong 250102, P.R. China

Received March 14, 2023; Accepted December 18, 2023

DOI: 10.3892/etm.2024.12433

Abstract. Thoracic aortic aneurysms (TAAs) are a major cause of death owing to weaker blood vessel walls and higher rupture rates in affected individuals. Vascular smooth muscle cells (VSMCs) are the predominant cell type within the aortic wall and their dysregulation may contribute to TAA progression. Enhancer of zeste homolog 2 (EZH2), a histone methyltransferase, is involved in several pathological processes; however, the biological functions and mechanisms underlying VSMC phenotype transition and vascular intimal hyperplasia remain unclear. The present study aimed to determine the involvement of EZH2 in mediating VSMC function in the development of TAAs. The expression of EZH2 was revealed to be elevated in patients with thoracic aortic dissection and TAA mouse model through western blotting and reverse transcription-quantitative PCR experiments. Subsequently, a mouse model was established using β-aminopropionitrile. *In vitro,* EdU labeling, Transwell assay, wound healing assay and hematoxylin-eosin staining revealed that knocking down the *Ezh2* gene could reduce the proliferation, invasion, migration, and calcification of mouse primary aortic smooth muscle cells. Flow cytometry analysis found that EZH2 deficiency increased cell apoptosis. Depletion of *Ezh2* in mouse primary aortic VSMCs promoted the transformation of VSMCs from a synthetic to a contractile phenotype. Using RNA-sequencing analysis, it was demonstrated that *Ezh2* regulated a group of genes, including integrin β3 (*Itgb3*), which are critically involved in the extracellular matrix signaling pathway. qChIP found *Ezh2* occupies the *Itgb3* promoter, thereby suppressing the expression of *Itgb3*. *Ezh2* promotes the invasion and calcification of VSMCs, and this promoting effect is partially reversed by co-knocking down *Itgb3*. In conclusion, the present study identified a previously unrecognized EZH2-ITGB3 regulatory axis and thus provides novel mechanistic insights into the pathophysiological function of EZH2. EZH2 may thus serve as a potential target for the management of TAAs.

Correspondence to: Professor Guohai Su, Department of Cardiovascular Medicine, Jinan Central Hospital, Shandong University, 44 Wenhua West Road, Jinan, Shandong 250102, P.R. China
E-mail: gttstg@163.com

Professor Wenqian Yu, Department of Cardiac Surgery, Research Center of Translational Medicine, Jinan Central Hospital Affiliated to Shandong First Medical University, 105 Jiefang Road, Jinan, Shandong 250013, P.R. China
E-mail: yuwenqian1988@163.com

*Contributed equally

Key words: thoracic aortic aneurysms, vascular smooth muscle cells, epigenetics, enhancer of zeste homolog 2, phenotypic switching

Introduction

A thoracic aortic aneurysm (TAA) is a severe condition characterized by localized dilation of the thoracic aorta that expands >50% of its normal diameter, with an increased risk of rupture. TAAs can eventually lead to thoracic aortic dissection (TAD), a life-threatening condition. It is estimated that 6-8 per 100,000 individuals are affected by the disease annually, and its incidence continues to rise worldwide (1,2). Globally, TAA is the most common cause of death and the second most prevalent aortic disease after atherosclerosis (3). Hypertension, atherosclerosis, diabetes mellitus, smoking and hypercholesterolemia are considered risk factors for TAA (4). Given this background, the lack of effective treatment options to prevent, treat or manage TAA is a major concern. The current treatment strategy for TAA primarily involves surgical interventions (5). In recent years, advances in high-throughput OMICS technologies, including genomics, transcriptomics, proteomics and metabolomics, have provided novel insights into the molecular mechanisms underlying the development and progression of TAA (2). The discovery and development of novel and effective therapeutic interventions for the prevention and treatment of TAA are of significant importance to public health.

The aortic wall is comprised of an organized architecture of different concentric layers consisting of cells and the extracellular matrix (ECM). The ECM consists of a diverse array of proteins, glycoproteins and proteoglycans, forming a dynamic microenvironment that provides structural support, mechanical strength and biochemical cues to cells (6).

Notably, the ECM also functions as a signaling platform that regulates cellular behavior, including proliferation, migration, differentiation and apoptosis (7). Dynamic ECM remodeling plays a crucial role in cardiovascular disease, including remodeling of cardiac hypertrophy, atherosclerosis and plaque formation (8). Understanding the intricate interactions within the ECM signaling pathway could potentially provide novel strategies for treating and managing cardiovascular diseases. Vascular smooth muscle cells (VSMCs) are the primary cells that compose the vascular wall tissue, and maintain vascular tension and mechanotransduction (3). Although the pathogenetic mechanisms of TAA remain to be fully elucidated, the development of this vascular disease is characterized by disruption of the ECM and VSMC phenotypic switching (9). In healthy blood vessels, most VSMCs are quiescent, contractile and proliferate slowly; however, following certain injuries, VSMCs change their phenotype in the presence of several injurious stimuli, switching from a contractile to a synthetic, migrating and proliferating phenotype (3), in a process termed VSMC phenotypic switching. Numerous studies have identified a strong relationship between VSMC phenotypic switching and atherosclerosis (10-12). The ECM contributes to providing resilience and tensile strength to tissues through elastic and collagen fibers (13). Moreover, the ECM contributes to the structural integrity of the vessel wall, which primarily consists of elastin, collagen, glycoproteins and proteoglycans (6). The ECM provides tensile strength and elasticity to vessel walls and regulates several processes, including proliferation, migration, differentiation and adhesion of VSMCs (3,6). An imbalance between anabolic (ECM synthesis) and catabolic (ECM degradation) phases in the composition of the ECM can result in the development of aortic aneurysms (14).

Epigenetic regulation also participates in VSMC phenotypic switching and disruption of the ECM (2). Epigenetic modification refers to a genetic change that involves gene function or gene expression but is unrelated to the DNA sequence (15). Numerous recent studies have shown several epigenetic signs of TAA that are correlated with chromatin alterations, including local DNA hypermethylation, altered histone methylation/demethylation (16) and histone acetylation/deacetylation balance (17). Enhancer of zeste homolog 2 (EZH2) is a histone methyltransferase that di- and tri-methylates H3 at lys27 (H3K27me2 and H3K27me3) to suppress gene transcription (6,18). One study has shown that EZH2 plays a key role in the physiology, pathology and development of the cardiovascular system (18). It maintains the integrity of the developing vasculature by inhibiting the expression of *Creb3l1*, *Fosl1*, *Klf5* and *Mmp9*. Wang *et al* (19) demonstrated that EZH2 expression increases the migration of pulmonary arterial smooth muscle cells (SMCs) and participates in the pathogenesis of pulmonary arterial hypertension. EZH2 enhances apoptosis in SMCs and the formation of abdominal aortic aneurysms (20). However, the biological effects of EZH2, as well as the association between EZH2 and TAA, remain unclear.

The present study explored the role of EZH2 in the occurrence of TAA and its impact on the phenotypic transformation of VSMCs. Using RNA sequencing and qChIP, the current study sought to identify the signaling pathways directly regulated by *Ezh2* and key target genes, further investigating the effect of the *Ezh2*-target gene axis on smooth muscle cell invasion and calcification. This study provides a valuable foundation for further research into the molecular mechanisms of TAA, highlighting the potential for targeted EZH2 therapy for TAA.

Materials and methods

Antibodies and reagents. The following antibodies were used at the stated dilutions in the present study: Anti-EZH2 (1:1,000; cat. no. 5246; Cell Signaling Technology, Inc.), anti-ITGB3 (1:1,000; cat. no. 18309-1-AP; ProteinTech Group, Inc.), anti-β-actin (1:50,000; cat. no. 3700S; Cell Signaling Technology, Inc.), anti-GAPDH (1:100,000; cat. no. 5174; Cell Signaling Technology, Inc.), anti-MMP2 (1:1,000; cat. no. 10373-2-AP; ProteinTech Group, Inc.), anti-MMP9 (1:1,000; cat. no. 13667S; Cell Signaling Technology, Inc.), anti-transgelin (TAGLN; 1:1,000; cat. no. ab14106; Abcam), anti-α-smooth muscle actin (α-SMA; 1:1,000; cat. no. 19245T; Cell Signaling Technology, Inc.), anti-cleaved caspase 3 (1:1,000; cat. no. 9664; Cell Signaling Technology, Inc.), anti-caspase 8 (1:1,000; cat. no. ab25901; Abcam), anti-Fas (1:1,000; cat. no. 4233; Cell Signaling Technology, Inc.) and anti-Bax (1:10,000; cat. no. 50599-2-Ig; ProteinTech Group, Inc.).

Cell culture and transfection. The aortic VSMCs used in the present study were derived from 4-week-old C57BL/6J wild-type littermate control mice who are the same as those in the 'Mouse model' using an explant technique (21). The method of mice sacrifice was the same method used in the 'Mouse model' subsection. After the mice were anesthetized by intraperitoneal injection of 400 mg/kg 10% chloral hydrate without peritonitis to minimize pain and discomfort, they were euthanized by cervical dislocation. The aorta was first separated from the arch, and the surrounding adipose tissue was stripped as much as possible. The media of the aorta were then dissected under a microscope and cut into 1-2 mm sections in PBS. Subsequently, VSMCs would move out of the finely divided media of the aorta tissue in DMEM (cat. no. A5669401; Gibco; Thermo Fisher Scientific, Inc.) supplemented with 10% FBS (cat. no. 11965118; Gibco; Thermo Fisher Scientific, Inc.) and 1% penicillin/streptomycin (cat. no. 1514022; Gibco; Thermo Fisher Scientific, Inc.). All cells were maintained in a humidified incubator with 5% CO_2 at 37˚C. Transfections were performed using Lipofectamine® RNAiMAX (Invitrogen; Thermo Fisher Scientific, Inc.) according to the manufacturer's protocol. Subsequently, 7-10x10^4 VSMCs were transfected with 100 nM small interfering (si)RNA, and the cells were collected immediately after transfection at 37˚C for 48 h to extract RNA and protein.. Each experiment was performed at least three times as biological triplicates. For RNA interference experiments, three independent siRNA sequences were tested for each gene. The sequences of the siRNAs used were: siEzh2-1, forward 5'-CAGCUCAAGAGGUUCAGAATT-3' and reverse 5'-UUCUGAACCUCUUGAGCUGTT-3'; siEzh2-2, forward 5'-GCACAAGUCAUCCCGUUAATT-3' and reverse 5'-UUA ACGGGAUGACUUGUGCTT-3'; siEzh2-3, forward 5'-CAA CACCCAACACAUAUAATT-3' and reverse 5'-UUAUAU GUGUUGGGUGUUGTT-3'; siItgb3-1, forward 5'-GCCCAU

GUUUGGCUACAAATT-3' and reverse 5'-UUUGUAGCCAAACAUGGGCTT-3'; siItgb3-2, forward 5'-GCAGGCUACAGUAUGUGAUTT-3' and reverse 5'-AUCACAUACUGUAGCCUGCTT-3'; siItgb3-3, forward 5'-GCCGUGAAUUGUACCUACATT-3' and reverse 5'-UGUAGGUACAAUUCACGGCTT-3'; and negative control (non-targeting) siRNA, forward 5'-UUCUCCGAACGUGUCACGUTT-3' and reverse 5'-ACGUGACACGUUCGGAGAATT-3'. All siRNAs were obtained from MilliporeSigma. Three independent siRNA sequences for Ezh2 and Itgb3 were effective. In the western blotting experiment, three siRNAs were all selected, and in the phenotypic transformation experiment the most efficient siRNA (siEzh2-1 and siItgb3-1) were selected.

Reverse transcription-quantitative PCR (RT-qPCR). Total RNA was extracted from the patient and mouse samples or VSMCs using TRIzol® reagent (Invitrogen; Thermo Fisher Scientific, Inc.) according to the manufacturer's protocol. Potential DNA contamination was removed by treating the RNA extraction products with RNase-free DNase (Promega Corporation). cDNA, used as the qPCR template, was generated from mRNA using MMLV Reverse Transcriptase according to the manufacturer's protocol (Roche Diagnostics GmbH). To amplify the cDNA, 1 μl forward and reverse primers (5 μM each) were mixed with 5.5 μl RNase-free water, 7.5 μl 2X SYBR Green Mix buffer (Toyobo Life Science) and 1 μl cDNA. The qPCR thermocycling conditions were: Initial denaturation at 95˚C for 10 min, followed by 40 cycles at 95˚C for 15 sec and 60˚C for 1 min. The relative quantification of all transcripts was detected using the RT-qPCR PRISM ABI 7500 rapid sequence detection system (Applied Biosystems; Thermo Fisher Scientific, Inc.). The fold changes were calculated using the $2^{-\Delta\Delta Cq}$ method (22). Mouse and human Gapdh were used as an internal control. Determinations were independently performed at least three times. The following primer pairs (all from Sangon Biotech, Co., Ltd.) were used for qPCR: *Gapdh*, forward 5'-AGGTCGGTGTGAACGGATTTG-3' and reverse, 5'-GGGGTCGTTGATGGCAACA-3'; *Ezh2*, forward 5'-AGCACAAGTCATCCCGTTAAAG-3' and reverse 5'-AATTCTGTTGTAAGGGCGACC-3'; *Ccnd2*, forward 5'-GAGTGGGAACTGGTAGTGTTG-3' and reverse 5'-CGCACAGAGCGATGAAGGT-3'; *Agtr1a*, forward 5'-TTGTCCACCCGATGAAGTCTC-3' and reverse 5'-AAAAGCGCAAACAGTGATATTGG-3'; *Cldn1*, forward 5'-TGCCCCAGTGGAAGATTTACT-3' and reverse 5'-CTTTGCGAAACGCAGGACAT-3'; *Sele*, forward 5'-ATGAAGCCAGTGCATACTGTC-3' and reverse 5'-CGGTGAATGTTTCAGATTGGAGT-3'; *Itga8*, forward 5'-TGTCTGGCGTTCAACTTGGAT-3' and reverse 5'-TCCAGTGAGTAGCCGAAGTAG-3'; *Igf1*, forward 5'-CACATCATGTCGTCTTCACACC-3' and reverse 5'-GGAAGCAACACTCATCCACAATG-3'; *End2*, forward 5'-GCTGGATCTAACCCAAGGACA-3' and reverse 5'-GACAGCGGTTGCAGGTACTC-3'; *Itgb3*, forward 5'-GGCGTTGTTGTTGGAGAGTC-3' and reverse 5'-CTTCAGGTTACATCGGGGTGA-3'; *Efnb2*, forward, 5'-TTGCCCCAAAGTGGACTCTAA-3' and reverse 5'-GCAGCGGGGTATTCTCCTTC-3'; *Tnnt2*, forward 5'-CAGAGGAGGCCAACGTAGAAG-3' and reverse 5'-CTCCATCGGGGATCTTGGGT-3'; *Vcan*, forward 5'-TGGCCCAGAACGGAAATATCA-3' and reverse 5'-ACTAGCCCGGAGTTTGACCAT-3'; *Itga2*, forward 5'-TGTCTGGCGTATAATGTTGGC-3' and reverse 5'-TGCTGTACTGAATACCCAAACTG-3'; *Ednrb*, forward 5'-AAGCCACGCTGTCACTTCTC-3' and reverse 5'-GAGGAACGCATCAGACTGGA-3'; *Fasl*, forward 5'-CAGCCCATGAATTACCCATGT-3' and reverse 5'-ATTTGTGTTGTGGTCCTTCTTCT-3'; *Mmp2*, forward 5'-ACCTGAACACTTTCTATGGCTG-3' and reverse 5'-CTTCCGCATGGTCTCGATG-3'; *Mmp9*, forward 5'-GCAGAGGCATACTTGTACCG-3' and reverse 5'-TGATGTTATGATGGTCCCACTTG-3'; *Acta2*, forward 5'-CCCAGACATCAGGGAGTAATGG-3' and reverse 5'-TCTATCGGATACTTCAGCGTCA-3'; *Tagln*, forward 5'-CCAACAAGGGTCCATCCTACG-3' and reverse 5'-ATCTGGGCGGCCTACATCA-3'; *Itgb7*, forward 5'-ACCTGAGCTACTCAATGAAGGA-3' and reverse 5'-CACCGTTTTGTCCACGAAGG-3'; *Itgb8*, forward 5'-TGCATGTTGTAACGTCAAGTGA-3' and reverse 5'-GATGCTGACACATCAACCAGATA-3'; *Cd44*, forward 5'-TCGATTTGAATGTAACCTGCCG-3' and reverse 5'-CAGTCCGGGAGATACTGTAGC-3'; *Thbs2*, forward 5'-CTGGGCATAGGGCCAAGAG-3' and reverse 5'-GTCTTCCGGTTAATGTTGCTGAT-3'; *Itga6*, forward 5'-TGCAGAGGGCGAACAGAAC-3' and reverse 5'-CGTGCTGCCGTTTCTCATATC-3'; *Itgb6*, forward 5'-ATGGGGATTGAGCTGGTCTG-3' and reverse 5'-GACAGGTGGGTGAAATTCTCC-3'; *Vwf*, forward 5'-CTCTTTGGGGACGACTTCATC-3' and reverse 5'-TCCCGAGAATGGAGAAGGAAC-3'; and *Agrn*, forward 5'-GCGGTACTTGAAAGGCAAAGA-3' and reverse 5'-CTCCAAAGCCACCAATTACCA-3'; Gapdh, forward 5'-GGAGCGAGATCCCTCCAAAAT-3' and reverse 5'-GGCTGTTGTCATACTTCTCATGG-3'; Ezh2, forward 5'-AATCAGAGTACATGCGACTGAGA-3' and reverse 5'-GCTGTATCCTTCGCTGTTTCC-3'; Itgb3, forward 5'-GTGACCTGAAGGAGAATCTGC-3' and reverse 5'-CCGGAGTGCAATCCTCTGG-3'.

Western blotting. Total protein from the human aortic tissues and VSMCs was extracted using RIPA lysis buffer (cat. no. 89901; Thermo Fisher Scientific, Inc.) supplemented with a Protease Inhibitor Cocktail (cat. no. HY-k0010; MedChemExpress). The Pierce™ BCA Protein Assay Kit (Thermo Fisher Scientific, Inc.) was used to determine protein concentrations. For western blotting, 5X loading buffer was added to the protein sample after it had been subjected to high-temperature denaturation at 95˚C for 10 min. Samples (20 μg/lane) were then loaded on an 8% separating gel for resolving 80-100 KDa proteins or a 10% separating gel for resolving 20-80 KDa proteins, and samples were resolved using SDS-PAGE. Separated proteins were then transferred to PVDF membranes (cat. no. IPVH00010; MilliporeSigma), which were blocked in 5% non-fat milk for 1 h at 25˚C, followed by incubation with the primary antibodies overnight at 4˚C. The following day, membranes were washed and incubated with horseradish peroxidase-conjugated goat anti-mouse IgG (1:10,000; cat. no. A25012; Abbkine, Inc.) or mouse anti-rabbit secondary antibodies (1:10,000; cat. no. A25022; Abbkine, Inc.) for 1 h at 25˚C. An Immobilon Western HRP Substrate (cat. no. WBKLS0100; Millipore, Inc.) substrate was added, and the protein signals were visualized using X-ray exposure in a darkroom. Western blotting was semi-quantified using ImageJ (Java 1.8.0_345; National Institutes of Health).

RNA-sequencing (RNA-seq) analysis. Total RNA was extracted by using TRIzol® reagent (Invitrogen; Thermo Fisher Scientific, Inc.) according to the manufacturer's protocol. The concentration and integrity of RNA samples from mouse aortic SMCs treating with siRNAs against *Ezh2* and control oligonucleotides were assessed using an Agilent 2100 RNA nano 6000 Assay Kit (Agilent Technologies, Inc.). Sequencing libraries were generated using a VAHTS Universal V6 RNA-seq Library Prep Kit for Illumina (cat. no. NR604-01/02; Vazyme Biotech Co., Ltd.) according to the manufacturer's protocol; index codes were added to attribute sequences to each sample. Briefly, mRNA was purified from total RNA (1 mg) using poly-T oligo-attached magnetic beads. Then, fragmentation buffer was added to break the mRNA into short fragments. First-strand cDNA synthesis was performed using random hexamer primers and RNase H. Second-strand cDNA synthesis was subsequently performed using nuclease-free water buffer, dNTPs, DNA polymerase I and RNase H. The double-stranded cDNA was purified using AMPure P beads (Agilent Technologies, Inc.). The purified double-stranded cDNA was repaired at the end, a tail was added and the sequence was connected to a connector, then the fragment size was selected, and finally, the cDNA library was obtained by PCR enrichment. These libraries were sequenced on the Illumina sequencing platform (Illumina NovaSeq 6000 S4; Illumina, Inc.) and 150 bp paired-end reads were generated. The RNA concentration of the library was diluted to 10 nM. The fluorescence qPCR instrument (Bio-Rad CFX 96, Bio-Rad Laboratories, Inc.) was used to accurately quantify the effective concentration of the library (library effective concentration: 100 nM), using iQ SYBRGRN (Bio-Rad Laboratories, Inc.). The cluster generation and sequencing were performed on a NovaSeq 6000 S4 platform, using a NovaSeq 6000 S4 Reagent kit V1.5 (Illumina, Inc.). Genes with fragments per kilobase of exon per million fragments mapped (FPKM) values of ≤0 across all samples were excluded from the analysis. Differentially expressed genes (DEGs) screened from VSMCs using siRNAs against *Ezh2* and control oligonucleotides were selected based on the selection criteria of P<0.001 and fold-change >|1.5|.

Functional enrichment analysis. Gene Ontology (23,24) enrichment of DEGs was performed using a hypergeometric test, in which the P-values were calculated and adjusted as q-values, and the background data were the genes in the entire genome. GO terms with a q-value <0.05 were considered to be significantly enriched. GO enrichment analysis can be used to determine the biological functions of the DEGs. Kyoto Encyclopedia of Genes and Genomes is a database containing a collection of manually drawn pathway maps representing knowledge on the molecular interactions and reaction networks (25). KEGG enrichment of DEGs was performed using a hypergeometric test, in which the P-values were adjusted using multiple comparisons as q-values. KEGG terms with a q-value <0.05 were considered to be significantly enriched. The Rich Factor represents the ratio of the number of target genes to the total genes annotated in a pathway. A greater Rich Factor indicates greater intensity. The q-value represents the corrected P-value, ranging from 0-1; a lower q-value indicates greater intensity. Data were analyzed using R package clusterProfiler (version 4.1.0) (26). Gene Set Enrichment Analysis (GSEA) was performed using the R package clusterProfiler (version 4.1.0) (26).

ChIP, quantitative ChIP (qChIP) and ChIP-PCR. ChIP and qChIP experiments were performed using VSMCs. Briefly, a pre-clearance step was performed and $1x10^7$ cells were treated with 1% formaldehyde for 10 min at 25˚C, sonicated at 4˚C every 1 sec (ultrasound 12-15 times as one cycle and repeated for 10 cycles) and cross-linked. ChIP lysis buffer consisted of 50 mM Tris-HCl, 5 mM EDTA and 1% SDS was added to the cells. Then, the cells were incubated with 2-3 μg primary antibody against rabbit IgG (control) (cat. no. Ab313801; Abcam) and EZH2 (cat. no. 5246; Cell Signaling Technology, Inc.). For ChIP assays, 30 μl protein G magnetic beads (Thermo Fisher Scientific, Inc.) adding to the lysate-bound antibodies were sequentially washed in the following buffers: 1 ml ChIP buffer I (20 mM Tris-HCl, 1% Triton X-100, 150 mM NaCl, 2 mM EDTA, 0.1% SDS), 1 ml ChIP buffer II (20 mM Tris-HCl, 1% Triton X-100, 500 mM NaCl, 2 mM EDTA, 0.1% SDS), and 1 ml ChIP buffer III (20 mM Tris-HCl, 1% w/v sodium deoxycholate, 0.25 M LiCl, 1 mM EDTA, 1% NP-40) for 5 min per wash at 4˚C. Next, the beads were washed with TE buffer (10 mM Tris-HCl, 1 mM EDTA) twice for 5 min at 4˚C. A total of 100 μl ChIP elution buffer (0.1 M $NaHCO_3$, 1% SDS) was added to each sample for 40 min at 37˚C; this step was repeated once. Finally, the ChIP eluent was placed in a constant temperature water bath at 65˚C for 12 h. qChIP was performed using 2X SYBR Green Mix buffer (Toyobo Life Science). PCR amplification was performed under the following: 94˚C for 3 min; 30 cycles of 94˚C for 30 sec, 55˚C for 40 sec, and 72˚C for 50 sec, followed by 72˚C for 5 min. After amplification, the products were separated in a 10% agarose gel containing 0.03% ethidium bromide and visualized using the FastGene FAS-DIGI PRO Gel imaging system. A NucleoSpin Gel and PCR Clean-up kit was used for DNA gel extraction according to the manufacturer's protocol (cat. no. 740609.50; Machery-Nagel GmbH). For ChIP-PCR assays, DNA template enrichment was performed using conventional PCR with primers specific to the target gene promoter. The following primer pairs were used for qChIP (Sangon Biotech, Co., Ltd.): *Gapdh*, forward 5'-TACTAGCGG TTTTACGGGCG-3' and reverse 5'-TCGAACAGGAGGAGC AGAGAGCGA-3'; *Itgb3*, forward 5'-CCATTGCACTGGGAT TAC-3' and reverse 5'-CTAGGCTACATAACAGGAAAG T-3'; *Efnb2*, forward 5'-GGACTGTGCCTTCCACCTAC-3' and reverse 5'-AACCACGGCTGTGACTTCTAC-3'; *Tnnt2*, forward 5'-TCAGAGGCTCGTGAAGTG-3' and reverse 5'-GGGAACAGGCTTGTAACATA-3'; *Vcan*, forward 5'-TAA CTGTTTGACCCTTTGC-3' and reverse 5'-CCCTACTCA GGCTTATCCA-3'; *Itga2*, forward 5'-CTTATTTCTGTCCCT TTCTCC-3' and reverse 5'-CAAGCCATAGCCCTCAAT-3'; *Ednrb*, forward 5'-TTTTGGTCCTTTGGGTGG-3' and reverse, 5'-TCCCGAAATCTGCTTGGT-3'; and *Fasl*, forward 5'-GGGAAGTGGGATGGATAG-3' and reverse 5'-GACCAA GGAGTTCGGCTA-3'.

Human aorta samples. Male patients aged 40-70 years old with TAD and coronary heart disease, who were diagnosed and received treatment at Jinan Central Hospital between May

2021 and July 2022, were recruited to the present study. The basic information on patients is listed in Appendix S1 and Table SI. Patients were excluded if they had other significant cardiovascular conditions, severe comorbidities, a history of previous aortic surgery or interventions, or known allergies, and/or were unable to provide informed consent. Only male patients aged 40-70 years with a clinically confirmed diagnosis that provided informed consent were included in the present study. The experimental group consisted of patients with TAD, who were treated with total aortic arch artificial vessel replacement, and frozen stent elephant trunk and mechanical aortic valve replacement. The control group consisted of patients with coronary heart disease (but who had healthy arteries) who received aortic arc-coronary artery bypass grafting. For further analysis, samples were either frozen immediately and stored at a temperature of -80˚C, or fixed overnight in 4% paraformaldehyde at 4˚C for staining.

For hematoxylin and eosin (H&E) staining, fixed samples were embedded in paraffin, sectioned into 4-μm slices, and stained with hematoxylin for 5 min at 25˚C followed by staining with eosin for 5 min at 25˚C. For elastica van Gieson (EVG) staining, the paraffin sections were immersed successively in Environmentally Friendly Dewaxing Transparent Liquid I (cat. no. G1128; Wuhan Servicebio Technology Co., Ltd.) for 20 min at 25˚C, Environmentally Friendly Dewaxing Transparent Liquid II (cat. no. G1128; Wuhan Servicebio Technology Co., Ltd.) for 20 min at 25˚C , anhydrous ethanol I for 5 min at 25˚C, anhydrous ethanol II for 5 min at 25˚C and 75% alcohol for 5 min at 25˚C, followed by washing with tap water at 25˚C. The EVG dye set utilized was (cat. no. G1042) from Wuhan Servicebio Technology Co., Ltd. EVG dye solution A, EVG dye solution B and EVG dye solution C were mixed in a ratio of 5:2:2 to form the EVG dye solution, prepared 2 days in advance. The sections were immersed in the EVG dye solution for 5 min at 25˚C and then rinsed with tap water. EVG dye B was diluted twice to 5% concentration after slight differentiation, and the sections were washed with tap water. This process was repeated under microscopic control until the elastic fibers appeared purplish-black, the background turned gray and nearly colorless. To form VG dye, 9 ml of EVG dye E and 1 ml of EVG dye D were mixed. The sections were dyed for 1-3 min at 25˚C, depending on the tissue's elastic fiber composition. Rapid water washing ensued, followed by three rounds of 100% anhydrous ethanol for rapid dehydration. Xylene was used for transparency for 20 sec, repeated twice for 5 min each (xylene exclusive, not shared with other xylene) at 25˚C. The sections were finally sealed with neutral gum. Light microscopy was employed for image acquisition and analysis, revealing purplish-black elastic fibers, red collagen fibers and a yellow background.

Immunohistochemistry staining. The sections were sequentially treated with environmentally friendly dewaxing solution I for 10 min at 25˚C, environmentally friendly dewaxing solution II for 10 min at 25˚C, environmentally friendly dewaxing solution III for 10 min and anhydrous ethanol I, II and III for 5 min at 25˚C each, followed by distilled water at 25˚C. The slices were subjected to repair using EDTA (pH 8.0; cat. no. G1206; Wuhan Servicebio Technology Co., Ltd.) in a microwave at medium heat (wattage at 400 W) for 9 min, followed by an 8-min cooling period, and then a 7-min cycle at medium-low heat (wattage at 300 W). After the repair process, the slices were allowed to cool naturally. Subsequently, the glass slides were placed in PBS (pH 7.4) and shaken on a decolorizing shaking table for three wash cycles, each lasting 5 min at 25˚C. The sections were then immersed in a 3% hydrogen peroxide solution and incubated at room temperature away from light for 25 min. Subsequently, the slides were placed in PBS (Ph 7.4) and washed three times on a decolorizing shaking table for 5 min each at 25˚C. To block non-specific binding, the tissue was uniformly covered with 3% BSA (cat. no. GC305010; Wuhan Servicebio Technology Co., Ltd.) in the tissue chemical circle and left at room temperature for 30 min. After gently shaking off the sealing solution, PBS and the primary antibodies anti-SMA (1:1,000; cat. no. NB300978; Novus Biologicals Co., Ltd.) or anti-EZH2 (1:1,000; cat. no. A11085; ABclonal Biotech Co., Ltd.) were added to the sections, which were then placed flat in a wet box at 4˚C for overnight incubation. The following day, the slides were placed in PBS (pH 7.4) and washed by shaking on the decolorizing shaker for three times, 5 min each at 25˚C. After slight drying of the sections, the tissue was covered with the secondary antibodies HRP-labeled goat anti-rabbit IgG (1:1,000; cat. no. GB23303; Wuhan Servicebio Technology Co., Ltd.) or FITC-labeled donkey anti-goat IgG (1:200; cat. no. GB22404; Wuhan Servicebio Technology Co., Ltd.), and incubated at room temperature for 50 min. The slides were washed in PBS (pH 7.4) on the decolorizing table for three times, 5 min each at 25˚C. Following slight drying, freshly prepared DAB color developing solution was added into the circle, and the color developing time was controlled under the microscope ~30 sec at 25˚C. Positive coloration appeared as brown and yellow, and the sections were rinsed with tap water to terminate the color development. Hematoxylin (cat. no. G1004; Wuhan Servicebio Technology Co., Ltd.) re-staining was performed for ~3 min at 25˚C, followed by washing with tap water, and hematoxylin differentiation solution (cat. no. G1039; Wuhan Servicebio Technology Co., Ltd.) was applied for ~10 sec at 25˚C. After hematoxylin (cat. no. G1004; Wuhan Servicebio Technology Co., Ltd.) re-staining for ~3 min at 25˚C, the sections were washed with tap water. Subsequently, hematoxylin differentiation solution (cat. no. G1039; Wuhan Servicebio Technology Co., Ltd.) was applied for ~30 sec at 25˚C, followed by rinsing with tap water. The sections were then treated with hematoxylin return to blue solution (cat. no. G1040; Wuhan Servicebio Technology Co., Ltd.) for ~30 sec at 25˚C and rinsed. The slices were immersed successively in 75% alcohol for 5 min at 25˚C, 85% alcohol for 5 min at 25˚C, anhydrous ethanol for 5 min, anhydrous ethanol for another 5 min at 25˚C, n-butanol for 5 min and xylene for 5 min at 25˚C to undergo dehydration and achieve transparency. After briefly drying the slices, they were taken out of xylene and sealed with neutral gum (cat. no. WG10004160; Wuhan Servicebio Technology Co., Ltd.). The interpretation of results was conducted under a white light microscope (Leica Microsystems GmbH). Immunohistochemistry staining was semi-quantified using ImageJ (Java 1.8.0_345; National Institutes of Health).

Mouse model. A total of 12 C57BL/6J male mice 4-week-old male mice (~20 grams each; Pengyue Experimental Animal

Breeding Co., Ltd) were divided into two groups of six mice each. The TAD model was induced by administering β-aminopropionitrile (BAPN; 1 g/kg/day; cat. no. A3134-25G; Sigma-Aldrich; Merck KGaA) in drinking water or an equivalent amount of saline as control group for 4 weeks, as previously described (27). All mice were housed in a clean and well-ventilated cage with appropriate bedding material, access to fresh water and food, a controlled environment with a temperature range of 20-26˚C and humidity maintained between 40-60%, in a specific pathogen-free environment with a 12-h light-dark cycle. Mice were anesthetized via intraperitoneal injection of 10% chloral hydrate (400 mg/kg), without signs of peritonitis, pain or discomfort, and were euthanized by cervical dislocation.

Flow cytometry. Cells were resuspended in sorting buffer [1X PBS, 3% FBS (v/v), and 3 mM EDTA (v/v)] before analysis. VSMCs were incubated with Annexin V-FITC and PI solutions for 20 min at 25˚C in the dark. The samples were then subjected to flow cytometric analysis (BD FACSverse Flow Cytometer; BD Biosciences). Subsequent data analyses were performed using FlowJo version 9.2 (FlowJo LLC).

EdU incorporation assay. For the EdU incorporation assay, a Click-iT™ Edu Cell Proliferation kit was used. VSMCs cells were seeded at a density of 3-5x10^4 cells/well in 12-well plates with glass slides in each well. Cells were then treated with siRNAs which were diluted to a working concentration of 100 nM. The medium was replaced with normal medium after 8 h, and the cells were subsequently cultured for an additional 24 h. EdU solution Alexa Fluor™ 488 dye (Invitrogen; Thermo Fisher Scientific, Inc.) was added to the medium for the last 3 h of the 24 h incubation period. Then, the cells were fixed with 4% paraformaldehyde for 30 min at 25˚C and incubated with 2 mg/ml glycine for 5 min at 25˚C to neutralize paraformaldehyde. Cells were incubated with 1X Apollo staining solution (Invitrogen; Thermo Fisher Scientific, Inc.) for 30 min at 25˚C in the dark after washing with PBS containing 0.5% Triton X-100 for 10 min. Next, the cells were washed again with 0.5% Triton X-100 PBS solution and incubated with 1X Hoechst 33342 for 30 min at room temperature in the dark. Finally, the cells were washed three times with PBS. Fluorescent images of the cells were obtained using a fluorescence microscope (Leica Microsystems GmbH).

Cell invasion assay. Transwell chamber filters (MilliporeSigma) were coated with Matrigel (Becton, Dickinson and Company) at 37˚C for 2 h and used for cell invasion assays. Subsequently, Ezh2 knockdown cells were resuspended in serum-free medium and pipetted into the upper chamber of the 8.0 μm pore size Transwell system (3x10^4 cells/0.5 ml serum-free medium). The lower chamber was filled with 500 μl medium supplemented with 10% FBS and incubated for 18-24 h at 37˚C. Next, cotton swabs were used to remove the cells that had not invaded, followed by staining of the membrane with crystal violet for 30 min at 25˚C. The images were captured and the number of cells that had invaded was counted. Each membrane was divided into three visual fields and the cells were counted using a light microscope.

Wound healing assay. Ezh2 knockdown cells and the respective negative control cells were seeded in 6-well dishes and grown to 80% confluence. A linear wound was introduced using a 200-μl pipette tip to scratch along the sub-confluent cell monolayer, and the debris were washed away with PBS. The cells were subsequently incubated in DMEM without FBS. Images were captured 0 and 24 h after scratching, and wound closure was semi-quantified using ImageJ (Java 1.8.0_345; National Institutes of Health). Images were captured using a light microscope. For the wound healing assay, three repeats were performed.

In vitro VSMC calcification. VSMC calcification was induced in osteogenic media containing 0.25 mM L-ascorbic acid and 10 mM β-glycerophosphate (Sigma-Aldrich; Merck KGaA) with H_2O_2 (0.4 mM) for 3 weeks. Calcification was determined by Alizarin Red staining (cat. no. G1450; Beijing Solarbio Science & Technology Co., Ltd.) according to the manufacturer's protocol.

Statistical analysis. Data are presented as the mean ± SD of three independent experiments unless otherwise indicated. Statistical comparisons were performed using a two-tailed unpaired Student's t-test or a one-way ANOVA for normally distributed variables. F-testing was used to test homogeneity of variance. If equal variance was not assumed, unpaired t-tests with Welch' s correction or Welch ANOVA tests were used. Differences among non-normally distributed variables were analyzed using the Mann-Whitney U-test or Kruskal-Wallis H-test. Statistical analyses were performed using GraphPad Prism version 8.0 (Dotmatics). $P<0.05$ was considered to indicate a statistically significant difference.

Results

EZH2 expression is upregulated in patients with TAD. To determine the potential involvement of EZH2 in the regulation of TAA progression, aortic wall specimens were collected from patients with TAD alongside control group consisted of patients with coronary heart disease at Jinan Central Hospital. H&E staining and elastica van Gieson (EVG) staining were used to visualize disordered and excessive proliferation of SMCs, which are hallmarks of TAD development (Fig. 1A and B). Western blotting and RT-qPCR were used to evaluate EZH2 expression in the aortic walls of patients with TAD, and they both showed that EZH2 expression was increased in the aortic samples of patients with TAD compared with the control samples (Fig. 1C and D). The immunohistochemistry and immunofluorescence staining for EZH2 showed a statistically significant increase in EZH2 expression in the aortic media of patients with TAD (Fig. 1E and F). Immunofluorescence analysis revealed that α-SMA protein was highly expressed in control group (Fig. 1F). These data suggested that EZH2 may be involved in TAD development.

Ezh2 expression is increased in the mouse model of TAA. To further confirm the association between EZH2 expression and TAA, a well-established experimental arterial aneurysm mouse model that was generated from wild-type C57BL/6J mice administered BAPN (1 g/kg/day) in drinking water

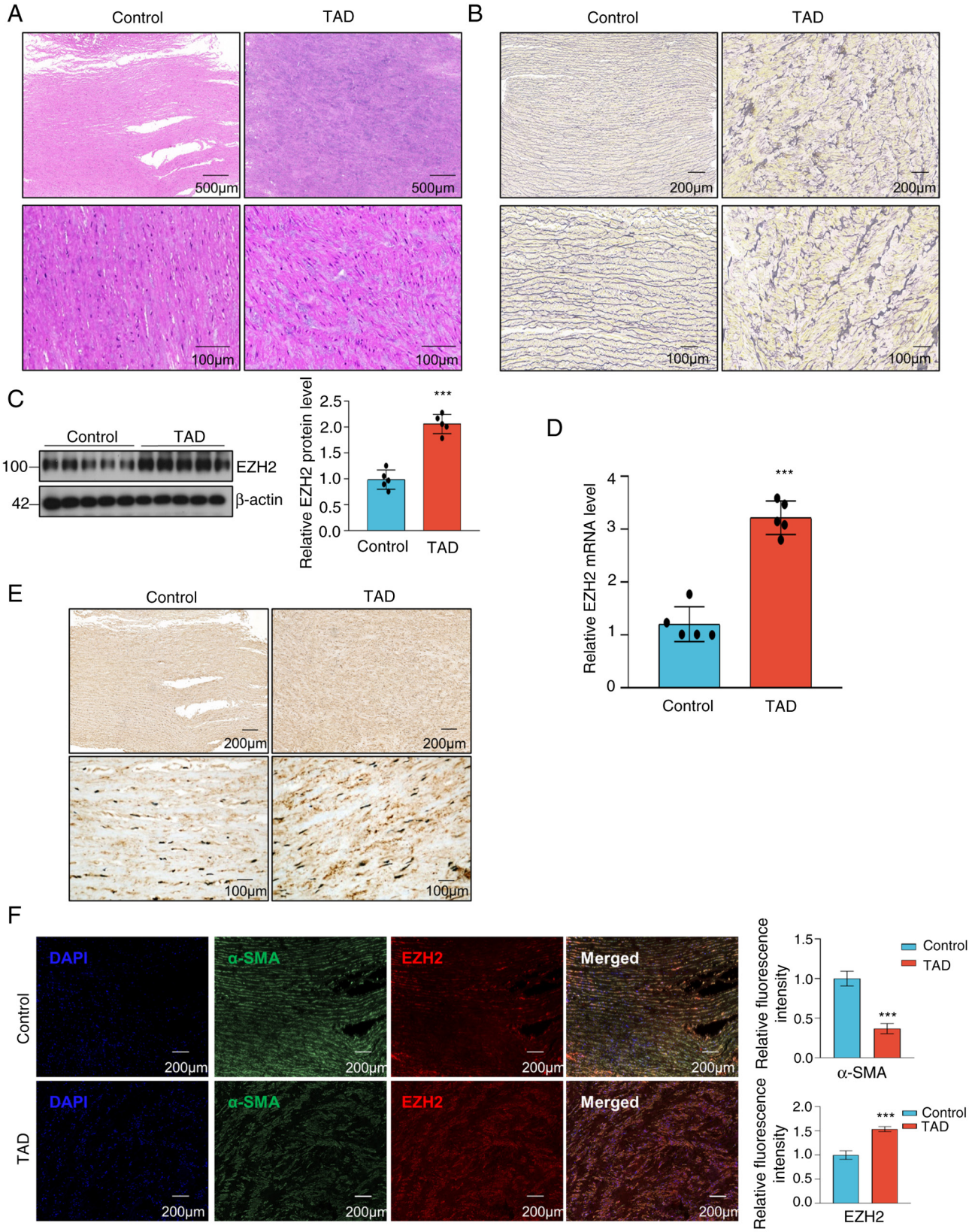

Figure 1. EZH2 expression is upregulated in specimens from patients with TAD. (A) Representative images of *he*matoxylin and eosin staining in the aortic media from patients with TAD and CHD. Scale bar, 500 or 100 μm. (B) Representative images of elastica van Gieson staining in the aortic media from patients with TAD and normal aortic tissues. Scale bar, 200 or 100 μm. (C) Western blot analysis of EZH2 protein in control aortic tissues and tissues from patients with TAD (n=5 for normal tissues and n=5 for TAD). β-actin served as an internal control. Semi-quantification analysis of EZH2 protein expression in the control aortic tissues and tissues from patients with TAD (n=5 for normal tissues and n=5 for TAD). (D) EZH2 expression in control aortic tissues or tissues of patients with TAD was determined using reverse transcription-quantitative PCR (n=5 for normal tissues and n=5 for TAD). (E) Representative images of immunohistochemical staining for EZH2 in aortic media from patients with TAD and normal aortic tissues. Scale bar, 200 or 100 μm. (F) Representative images of immunofluorescence staining in aortic media from patients with TAD and normal aortic tissues. Scale bar, 200 or 100 μm. Histogram showing the relative α-SMA and EZH2 fluorescence intensity. Data are presented as the mean ± SD of three independent experiments and were analyzed using a two-tailed unpaired Student's t-test. ***P<0.001 vs. Control. EZH2, enhancer of zeste homolog 2; TAD, thoracic aortic dissection; α-SMA, α-smooth muscle actin.

for 4 weeks or an equivalent amount of saline (control) was used (27). Given the anatomical changes, establishment of the model was considered successful (Fig. 2A). Consistently, H&E and EVG staining revealed that elastin breakage was markedly increased in TAA mice and the VSMCs were disorganized (Fig. 2B and C). Western blotting and RT-qPCR analyses showed that Ezh2 expression was increased in the aortic tissues of TAA mice when compared with control mice (Fig. 2D and E). Moreover, increased Ezh2 expression was detected in the aorta of TAA mice compared with in the control aorta (Fig. 2F). As observed by immunostaining, the experimental mice showed a significant increase in the positive expression of Ezh2 and minimal expression of α-Sma in aortic tissues compared with the control mice (Fig. 2G). These results demonstrated that Ezh2 plays an essential role in the development of TAA in mice. Similarly, the expression of Ezh2 was higher in the aortic media of TAA mice, which is consistent with the findings in patients with TAD.

Ezh2 knockdown influences VSMC phenotypic switching. To determine the role of Ezh2 in VSMCs, a siRNA against Ezh2 was used to target Ezh2 expression. VSMCs were successfully isolated and cultured, which was confirmed by immunofluorescence staining for α-SMA and TAGLN (Fig. 3A). Whether Ezh2 regulated VSMC proliferation and apoptosis was next assessed. The knockdown efficiency of Ezh2 was verified at the RNA and protein level (Fig. 3B and C). An EdU incorporation assay was performed to assess cell proliferation, and fewer EdU-positive cells were detected in the Ezh2 knockdown group compared with in the negative control group (Fig. 3D). Furthermore, to explore the effect of Ezh2 on VSMC apoptosis, western blot analyses were used to detect the expression levels of apoptosis-related proteins. The knockdown of Ezh2 led to a significant increase in the expression levels of the apoptosis-related proteins caspase 8, Fas, Bax and caspase 3 (Fig. 3E). In addition, VSMC apoptosis was analyzed through flow cytometry. The results showed a difference in the early and late apoptotic periods between the control and siRNA-mediated knockdown groups; notably, Ezh2 knockdown increased apoptosis (Fig. 3F). These results suggested that Ezh2 increases the capacity of VSMCs to proliferate and reduced VSMC apoptosis.

As VSMC proliferation is often associated with migration and phenotypic switching, the effects of Ezh2 on VSMC migration and phenotype were assessed to determine if Ezh2 was associated with VSMC phenotypic switching. The Transwell invasion model was used to assess the impact of Ezh2 on VSMC invasion. The results indicated that compared with in the control group, Ezh2 knockdown markedly reduced VSMC invasion (Fig. 3G). Furthermore, in the wound healing assays, the siEzh2 cells exhibited slower wound closure compared with the control group ($P<0.001$; Fig. 3H). Therefore, these results demonstrated that Ezh2 positively regulates VSMC invasion and migration.

The phenotypic transition of VSMCs is characterized by decreased expression of contractile markers, a key event contributing to VSMC proliferation and migration (14). Thus, the effect of Ezh2 on phenotypic VSMC switching was assessed. Knockdown of Ezh2 resulted in increased expression of contractile RNA markers, including *Acta2* (gene of α-SMA) and *Tagln*; however, the expression of synthetic RNA markers, including *Mmp2* and *Mmp9*, was decreased (Fig. 4A). Western blot analysis showed that *Ezh2* knockdown decreased the expression of the synthetic proteins MMP2 and MMP9 in the aortic tissues of TAA mice when compared with the control mice (Fig. 4B). The immunofluorescence assay also showed that the expression of both α-SMA and TAGLN was significantly increased in VSMCs with *Ezh2* expression knockdown (Fig. 4C). Ezh2 knockdown inhibited the calcification of VSMCs treated with the calcification medium (Fig. 4D). According to these data, Ezh2 directly promoted a proliferative and synthetic VSMC phenotype.

Genome-wide identification of EZH2 transcription targets. To determine how Ezh2 regulates TAA development, RNA-seq experiments were performed on mouse aortic SMCs using siRNAs against Ezh2 and control oligonucleotides. Compared with the control group, 758 upregulated genes and 614 downregulated genes were identified in the Ezh2 knockdown cells (Fig. 5A). GO analysis of the DEGs revealed that the dysregulated genes were involved in vital biological processes. Downregulated genes were enriched in pathways involving the 'PI3K-Akt signaling pathway', 'MAPK signaling pathway' and 'TNF signaling pathway' and included *Sele*, *Igf1*, *Edn1*, *Agtr1a* and *Gacna1g*, whereas upregulated genes were enriched in pathways that regulate cell adhesion molecules and ECM-receptor interaction, including *Itgb3*, *Vcan*, *Cd44*, *Itga2* and *Thbs2* (Fig. 5B). Based on the KEGG enriched pathways, the top 10 key biological processes were identified (Fig. 5C). To further investigate the biological significance of EZH2, Gene Set Enrichment Analysis (GSEA) was performed on differentially expressed EZH2 target genes and found a strong enrichment of the targets of cell adhesion molecule pathways. EZH2 is a key factor in the regulation of the ECM in TAD. GSEA results suggested that EZH2 may participate in the degradation of cell adhesion molecules, TNF and NF-κB signaling pathways, as well as lipids and atherosclerosis (Fig. 5D). Seven representative down or upregulated genes were further quantified by RT-qPCR using VSMCs to validate the RNA-seq results, which were enriched in several signal pathways related to VSMC functions (Fig. 5E). Considering that ECM is crucial for the phenotypic switching of VSMCs, it was found, using RNA-seq analysis, that EZH2 knockdown could indeed upregulate the expression of several well-known ECM markers, including *Itgb7*, *Itgb8*, *Cd44*, *Thbs2*, *Itga6*, *Itgb3*, *Itgb6* and *Agrn* (Fig. 5F). Subsequently, the upregulated DEGs in the ECM signal pathway were verified by RT-qPCR (Fig. 5G). In conclusion, based on these results, it was hypothesized that the epigenetic silencing of EZH2 is a key factor involved in ECM-receptor interactions.

Ezh2 regulates Itgb3 and participates in VSMC invasion and calcification. To further determine whether the target gene transcription was directly mediated by Ezh2 or not, the Ezh2 transcriptional targets were determined. qChIP assays using specific antibodies against Ezh2 showed strong binding to regions of *Itgb3*, but not to *Itga2*, *Vcan*, *Tnnt2*, *Efnb2*, *Fasl* and *Ednrb* (Fig. 6A). To verify this result, ChIP-PCR was used and it was found that Ezh2 bound to the promoter of the target gene *Itgb3* (Fig. 6B). The knockdown efficiency of *Itgb3* was

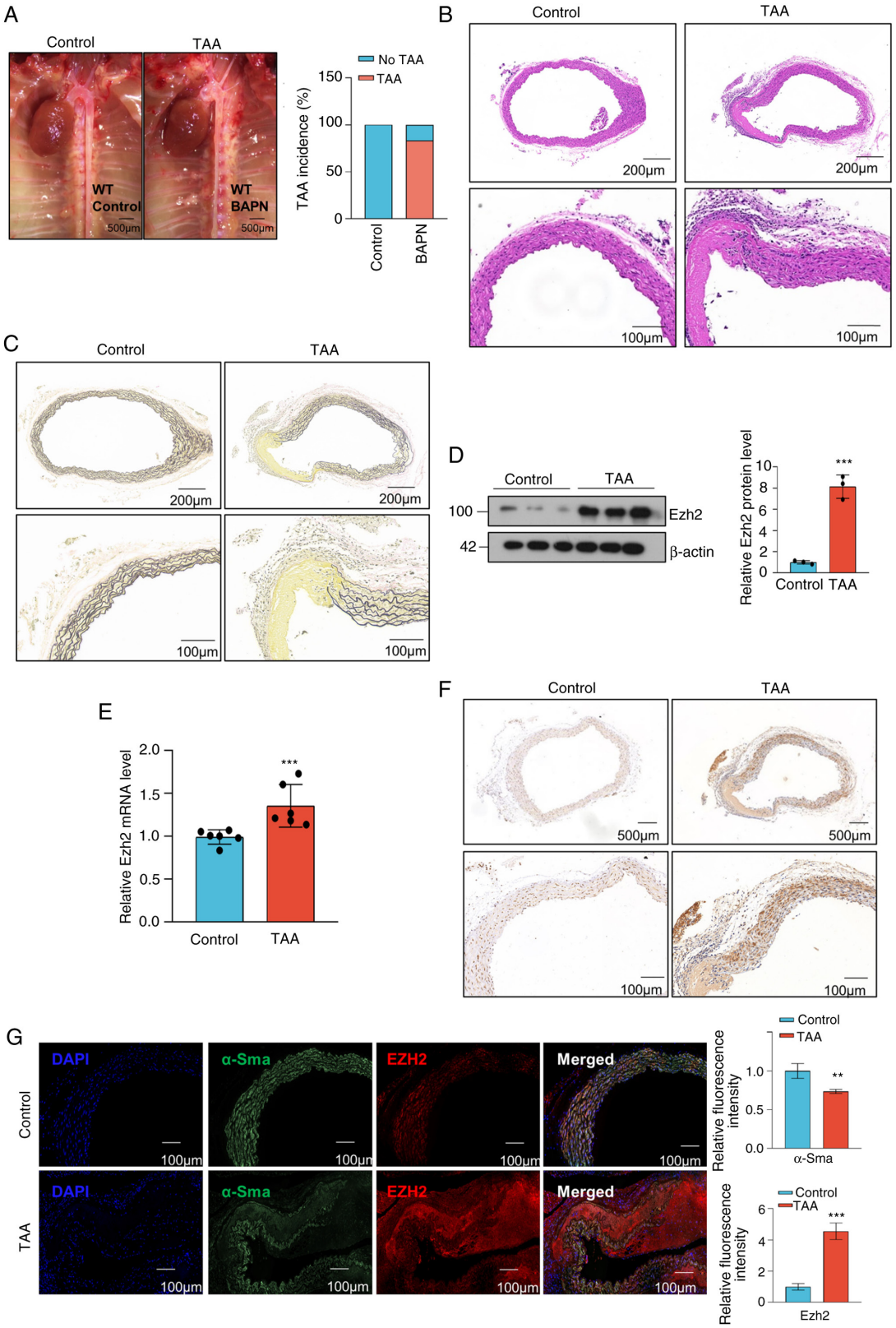

Figure 2. Ezh2 expression is upregulated in the TAA mouse model. (A) Representative anatomical images of the control and TAA mice. Scale bar, 500 μm. Quantification of the incidence of TAA in mice. (B) Representative images of hematoxylin and eosin staining in the aortic media of normal and TAA mice aortic tissues. Scale bar, 200 or 100 μm. (C) Representative images of elastica van Gieson staining in the aortic media of normal and TAA mice aortic tissues. Scale bar, 200 or 100 μm. (D) Western blot analysis of Ezh2 expression in the aortic tissues of normal and TAA mice (n=3 for normal tissues and n=3 for TAA). β-actin was used as the loading control. Densitometric analysis of EZH2 protein expression in the aortic tissues of normal and TAA mice (n=3 for normal tissues and n=3 for TAA). (E) Ezh2 expression in aortic tissues of normal and TAA mice was determined using reverse transcription-quantitative PCR (n=6 for normal tissues and n=6 for TAD). (F) Representative images of immunohistochemical staining for Ezh2 in aortic media of normal and TAA mice aortic tissues. Ezh2 expression was significantly upregulated in TAA mice tissues compared with the control mice. Scale bar, 500 or 100 μm. (G) Representative images of immunofluorescence staining in the aortic media of normal and TAA mice aortic tissues. Scale bar, 200 or 100 μm. Histogram showing the relative α-Sma and Ezh2 fluorescence intensity. Data are presented as the mean ± SD from three independent experiments and were analyzed using a two-tailed unpaired Student's t-test. **P<0.01 and ***P<0.001 vs. Control. EZH2, enhancer of zeste homolog 2; TAA, thoracic aortic aneurysms; α-SMA, α-smooth muscle actin.

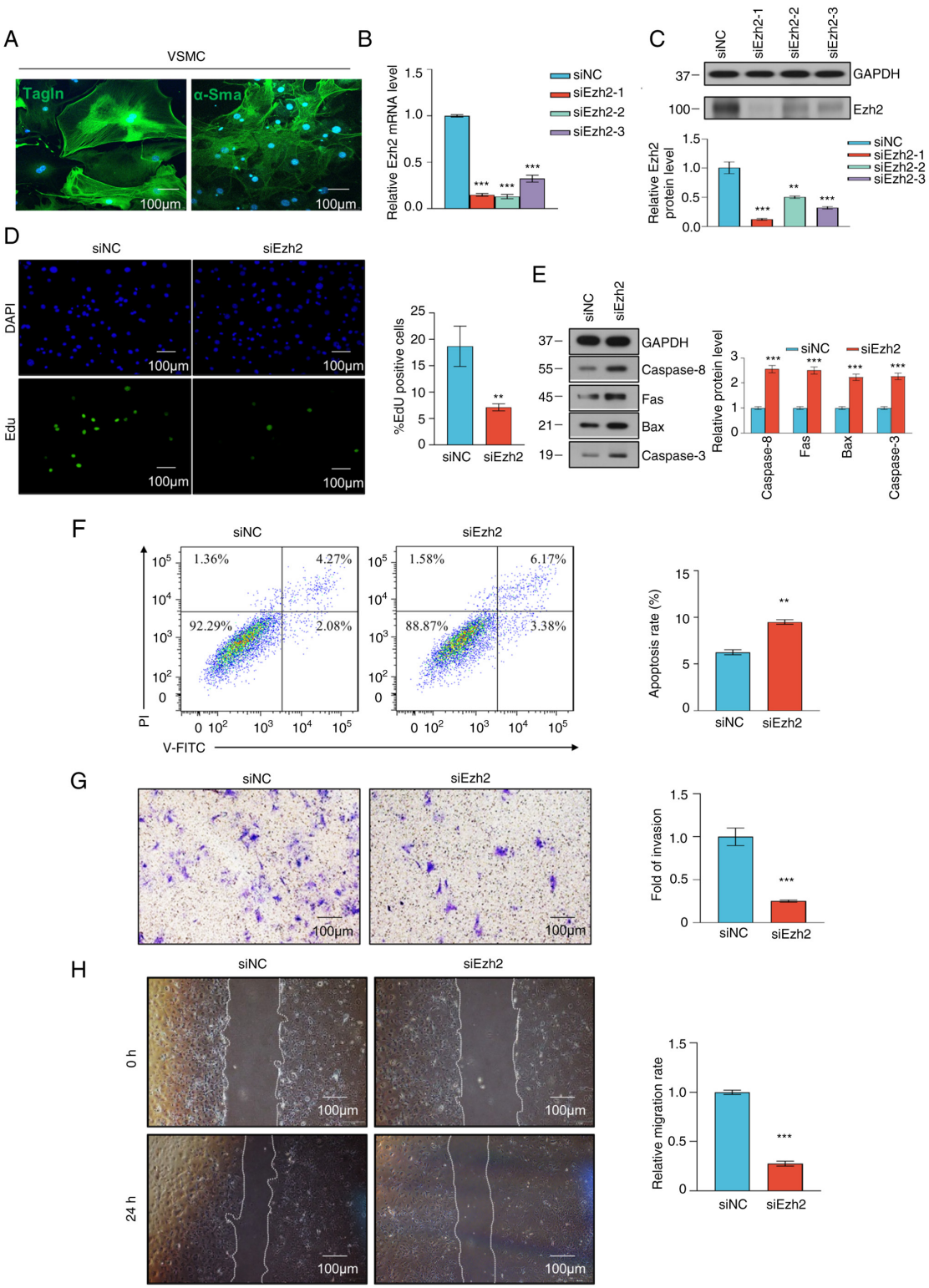

Figure 3. VSMC proliferation and migration were inhibited by Ezh2 knockdown. VSMCs were transfected with siNC or siEzh2. (A) Representative immunofluorescence staining of differentiation markers, Tagln and α-Sma in VSMCs. (B) Knockdown efficiency of Ezh2 was verified using reverse transcription-quantitative PCR. (C) Knockdown efficiency of Ezh2 was verified using western blotting. Gapdh was used as the internal control. Histogram showing the relative Ezh2 protein expression levels. (B and C) Data were analyzed using one-way ANOVA. (D) EdU proliferation assay analysis of the effect of Ezh2 on the proliferation of VSMCs. Cells exhibiting green fluorescence were in the S phase of mitosis. EdU proliferation assay was performed 24 h after transfection with siEzh2 and siNC. Scale bar, 100 μm). (E) Western blot analysis of apoptosis-related proteins in VSMCs 48 h post-transfection. Gapdh served as an internal reference. The histograms show the relative expression levels of apoptosis-related proteins in VSMCs at 48 h post-transfection. (F) Cells were stained with Annexin V-FITC and PI. Flow cytometry dot plots showing the percentage of stained cells. Histogram showing the percentage of Annexin V^+/PI^- and Annexin V^+/PI^+ of siNC-transfected and siEzh2-transfected VSMCs. (G) VSMC invasion was assessed using a Transwell assay of siNC-transfected and siEzh2-transfected VSMCs. Cells that had invaded were stained with crystal violet. Scale bar, 100 μm. Histogram showing the percentage of invading VSMCs. (H) Representative images of wound closure obtained 0 and 24 h after wounding in siNC-transfected and siEzh2-transfected VSMCs. Scale bar, 100 μm. Histogram showing the percentage of migrating cells in each group. (D-H) Data were analyzed using two-tailed unpaired Student's t-test. Data are presented as the mean ± SD of three independent experiments. **P<0.01, ***P<0.001 versus siNC groups. VSMC, vascular smooth muscle cell; EZH2, enhancer of zeste homolog 2; si, small interfering; NC, negative control; α-Sma, α-smooth muscle actin; Tagln, transgelin.

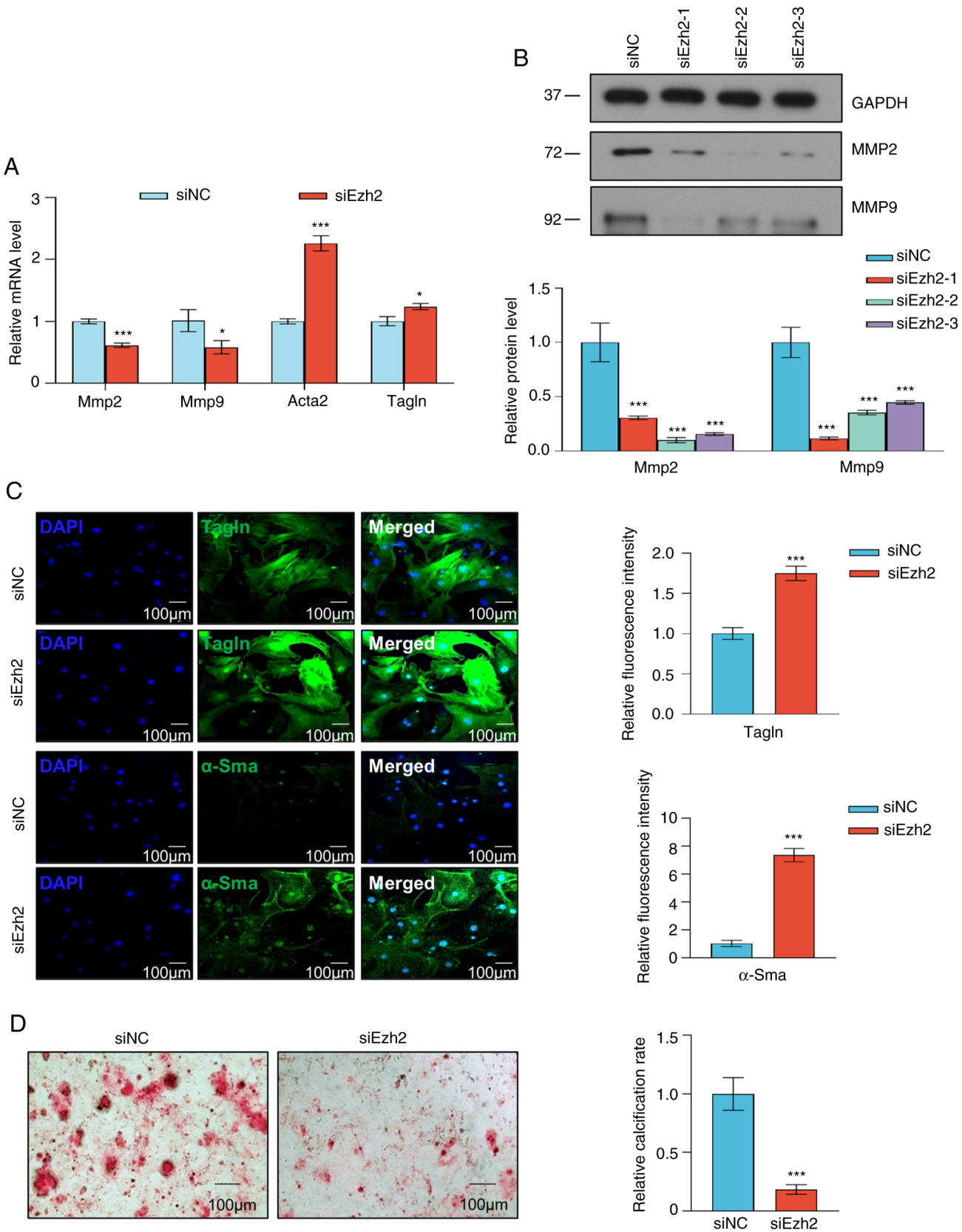

Figure 4. *Ezh2* knockdown influences VSMC phenotypic switching. (A) Expression of contractile markers (*Acta2* and *Tagln*) and synthetic markers (*Mmp2* and *Mmp9*) in siNC-transfected and siEzh2-transfected VSMCs for 48 h was determined using reverse transcription-quantitative PCR. Data were analyzed using two-tailed unpaired Student's t-test. (B) Western blot analysis of Mmp2 and Mmp9 expression in siNC-transfected and siEzh2-transfected VSMCs for 48 h. Gapdh was used as the loading control. Histogram showing the relative Mmp2 and Mmp9 protein expression levels. Data were analyzed using one-way analysis of variance. (C) Representative immunofluorescence staining for contractile markers (α-Sma and Tagln) in siNC-transfected and siEzh2-transfected VSMCs for 48 h. Histogram showing the relative α-Sma and Tagln fluorescence intensity. (D) Representative calcification images of siNC-transfected and siEzh2-transfected VSMCs for 48 h. Scale bar, 100 μm. Histogram showing the relative calcification rate. (C and D) Data were analyzed using two-tailed unpaired Student's t-test. Data are presented as the mean ± SD of three independent experiments *P<0.05, ***P<0.001 versus siNC groups. VSMC, vascular smooth muscle cell; EZH2, enhancer of zeste homolog 2; si, small interfering; NC, negative control; α-Sma, α-smooth muscle actin; Tagln, transgelin.

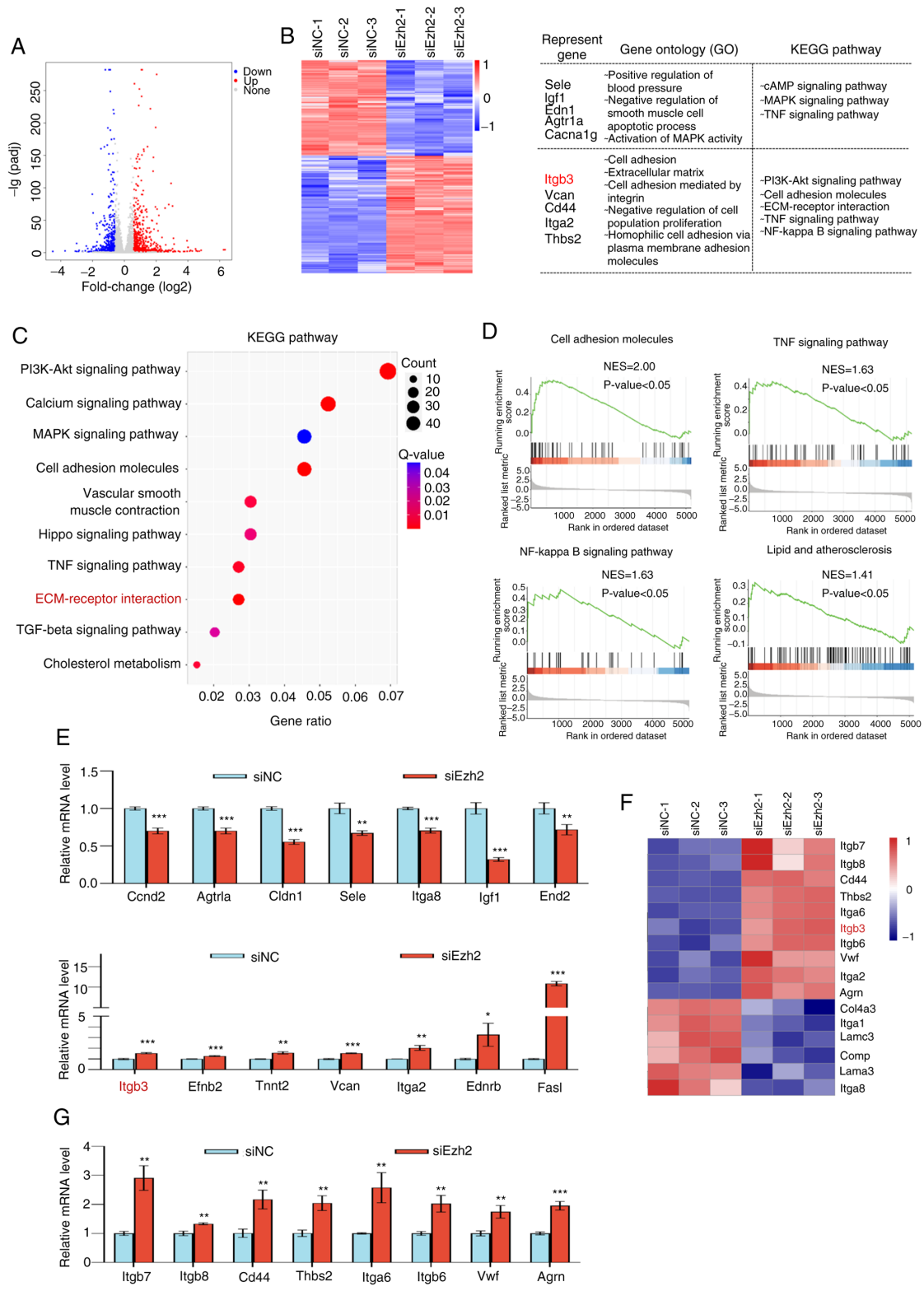

Figure 5. Genome-wide transcriptional target analysis for Ezh2. (A) Genomic distribution of Ezh2 targets based on RNA-seq analysis. (B) Heatmap of the differentially expressed genes (fold change >1.5; P<0.001) in control (siNC) and Ezh2 knockdown (siEzh2-1, siEzh2-2 and siEzh2-3) VSMCs. Red, upregulated genes; blue, downregulated genes. Results of the GO and KEGG pathway analyses of the differentially expressed genes. (C) A bubble chart of the top 10 enriched KEGG pathways. The Rich Factor represents the ratio of the number of target genes to the total genes annotated in a pathway. A greater Rich Factor indicates greater intensity. The q-value represents the corrected P-value, ranging from 0-1; a lower q-value indicates greater intensity. (D) Gene Set Enrichment Analysis plot of cell adhesion molecules, TNF signaling pathway, NF-κB signaling pathway, and lipid and atherosclerosis. (E) Verification of RNA-seq results using RT-qPCR analysis of selected genes in VSMCs. Results are expressed as the fold-change relative to the control. Gapdh was used as the negative control. (F) Heatmap of the differentially enriched ECM-receptor interaction pathway genes (fold change >1.5; P<0.001) in the control and Ezh2 knockdown (siEzh2-1, siEzh2-2 and siEzh2-3) VSMCs. Red, upregulated genes; blue, downregulated genes. (G) Verification of differentially expressed genes in the ECM signaling pathway using RT-qPCR in VSMCs. Results are expressed as the fold-change relative to Gapdh. Data are presented as the mean ± SD of three independent experiments and were analyzed using two-tailed unpaired Student's t-test. *P<0.05, **P<0.01, ***P<0.001 vs. siNC. EZH2, enhancer of zeste homolog 2; si, small interfering: NC, negative control; GO, Gene Ontology; KEGG, Kyoto Encyclopedia of Genes and Genome; ECM, extracellular matrix; NES, normalized enrichment score; RT-qPCR, reverse transcription-quantitative PCR.

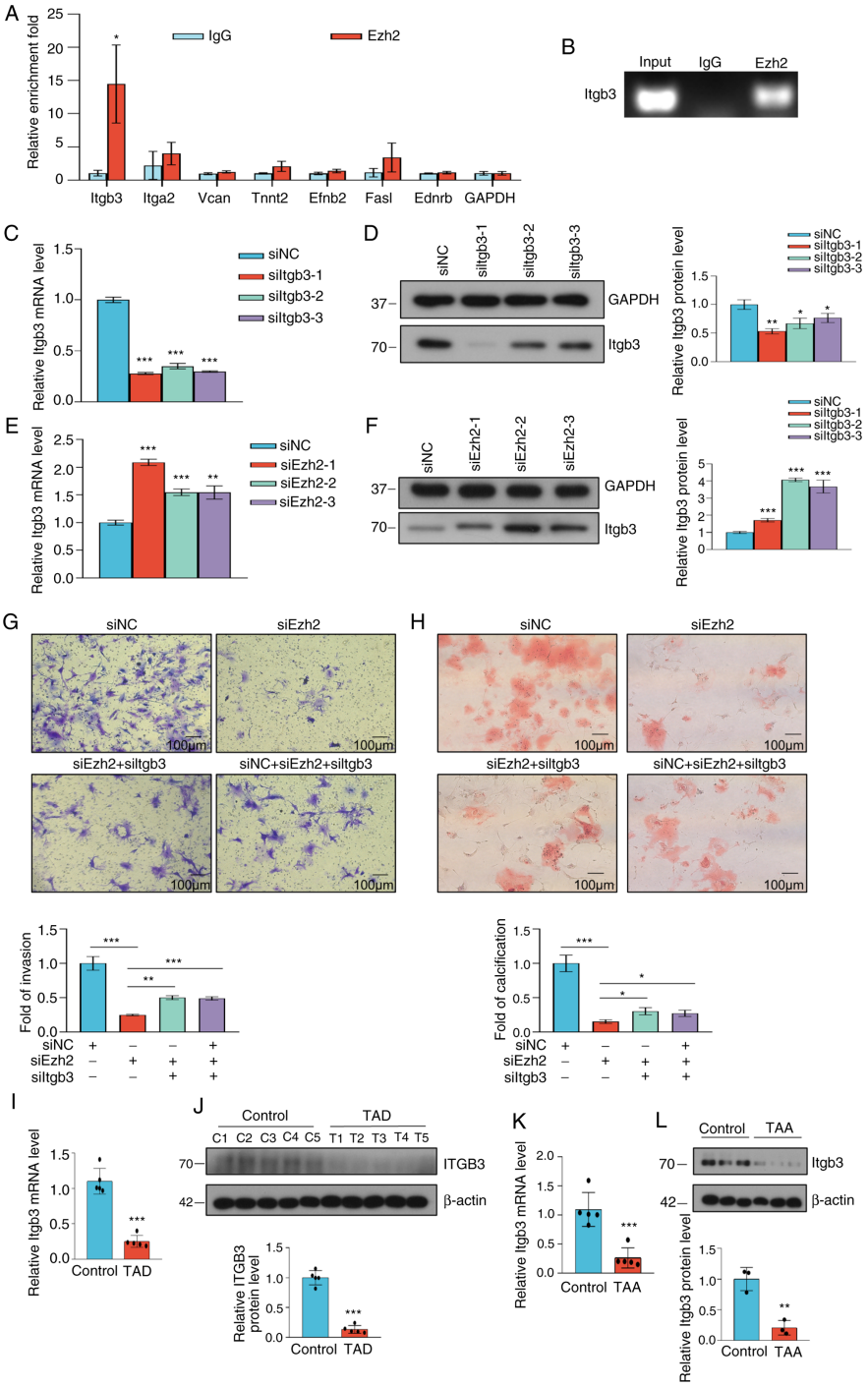

Figure 6. Ezh2 influences VSMC invasion and calcification by inhibiting Itgb3. (A) qChIP analysis of the selected genes in VSMCs. Results are presented as the enrichment fold relative to Gapdh. Data were analyzed using two-tailed unpaired Student's t-test. (B) ChIP-PCR results show Ezh2 binding on the promotor sites of Itgb3. (C) Knockdown efficiency of Itgb3 was verified using RT-qPCR. (D) Knockdown efficiency of Itgb3 was verified using western blotting. Histogram showing the relative Itgb3 protein level. (E) VSMCs were transfected with siNC or siEzh2. Itgb3 expression in VSMCs was detected 48 h post-transfection using RT-qPCR normalized to Gapdh. (F) Western blot analysis of Itgb3 expression in VSMCs 48 h post-transfection. β-actin was used as the loading control. Histogram showing the relative Itgb3 protein levels in VSMCs 48 h post transfection. (G) VSMC invasion was assessed using a Transwell assay using siNC-transfected, siEzh2-transfected, siEzh2 + siItgb3-transfected and siNC + siEzh2 + siItgb3-transfected VSMCs for 48 h. Cells that had invaded were stained with crystal violet. Scale bar, 100 μm. Histogram showing the fold of invading VSMCs. (H) Representative calcification staining of siNC-transfected, siEzh2-transfected, siEzh2 + siItgb3-transfected and siNC + siEzh2 + siItgb3-transfected VSMCs. Scale bar, 100 μm. Histogram showing the fold of calcified VSMCs. (C-H) Data were analyzed using one-way ANOVA. (I) ITGB3 expression in control aortic tissues or tissues of patients with TAD was determined using RT-qPCR (n=5 for normal tissues and n=5 for TAD). (J) Western blot analysis of EZH2 protein expression in control aortic tissues and tissues from patients with TAD (n=5 for normal tissues and 5 for TAD). β-actin was used as the loading control. Semi-quantification of ITGB3 protein expression in control aortic tissues and tissues from patients with TAD (n=5 for normal tissues and n=5 for TAD). (K) Itgb3 expression in aortic tissues of normal and TAA mice was determined using RT-qPCR (n=3 for normal tissues and n=3 for TAD). (L) Western blot analysis of Itgb3 in aortic tissues of normal and TAA mice (n=3 for normal tissues and n=3 for TAA). β-actin was used as the loading control. Semi-quantification of Itgb3 protein expression in the aortic tissues of normal and TAA mice (n=3 for normal tissues and n=3 for TAA). (I-L) Data were analyzed using two-tailed unpaired Student's t-test. Data are presented as the mean ± SD. *P<0.05 **P<0.01, ***P<0.001 versus control groups. EZH2, enhancer of zeste homolog 2; VSMC, vascular smooth muscle cell; qChIP, quantitative chromatin immunoprecipitation; si, small interfering; NC, negative control; RT-qPCR, reverse transcription-quantitative PCR; TAD, thoracic aortic dissection; TAA, thoracic aortic aneurysms.

verified at the RNA and protein levels (Fig. 6C and D). Each of the Ezh2 siRNAs led to a significant increase in the expression of Itgb3 at both the transcriptional (Fig. 6E) and protein levels (Fig. 6F). As previously stated, EZH2 plays an important role in VSMC calcification and invasion. Next, the role of Itgb3 in VSMCs was assessed. As determined using Transwell assays, *Ezh2* knockdown in VSMCs decreased cell invasion, which was partially rescued by *Itgb3* co-knockdown, indicating that Ezh2 could promote VSMC invasion through the suppression of Itgb3 (Fig. 6G). In parallel, compared with the control cells, knockdown of Itgb3 resulted in the partial rescue of the VSMC calcification ability that was decreased by Ezh2 knockdown (Fig. 6H). RT-qPCR and western blotting showed that Itgb3 expression was decreased in the aortic samples of patients with TAD ($P<0.001$; Fig. 6K and L) and the aortic tissues of TAA mice ($P<0.001$; Fig. 6M and N). These results suggested that Itgb3 may be a direct target of Ezh2 that plays a role in regulating VSMC invasion and calcification.

Discussion

TAA is the leading cause of death and morbidity worldwide, and it is especially challenging to manage due to the fragility of vessel walls and the high risk of rupture, resulting in a high mortality rate in affected individuals (1,2). TAA involves localized bulges or dilations of the aortic wall, whereas TAD involves a tear in the aortic lining that creates a false channel for blood flow. Both conditions require prompt medical evaluation and management to prevent serious complications. However, despite their differences, noteworthy similarities in the pathophysiological mechanisms and clinical presentations exist (28,29). The study of TAA and TAD may provide more effective insights into managing and addressing these complex and interrelated cardiovascular conditions. The etiology of TAA is heterogeneous as it can be influenced by both genetic and environmental factors, and environmental risk factors have been difficult to determine (2). Thus, epigenetic studies are necessary to overcome this limitation. Increasing evidence has shown that epigenetics plays a vital role in the pathological process of aortic media degeneration (30). The histone methyltransferase EZH2 is an enzymatically active subunit of the polycomb repressive complex, which di- and tri-methylates H3 at lys27 (H3K27me2 andH3K27me3) to suppress gene transcription. It has been implicated in various types of cancer, including prostate, thyroid, lung and bladder cancer, in which EZH2 promotes tumor cell proliferation and motility via epigenetic changes in cancer-associated gene expression levels (31,32). Furthermore, Mitić *et al* (33) showed that inhibition of EZH2 increases angiogenesis in ischemic tissue. However, whether EZH2 plays a role in VSMCs during TAA pathology, and whether this effect of EZH2 is related to the ECM pathway has not yet been determined. In the present study, when compared with control groups, EZH2 expression was significantly increased in the aortic wall of patients with TAD and in the mouse model of TAA. These findings are consistent with those of previous studies, with similar upregulated EZH2 expression observed in pulmonary hypertension and coronary heart disease (19,34). Ezh2 knockout has been shown to inhibit SMC proliferation and enhance apoptosis (12). Likewise, the results of the present study confirmed the regulatory role of Ezh2 in SMC proliferation (19,35). Furthermore, *Ezh2* occupied the *Itgb3* promoter and inhibited its expression, thereby promoting the invasion of VSMCs. Therefore, the results of the present study suggested that EZH2 regulates the phenotypic transformation of VSMCs by controlling ECM-related gene expression.

The aortic wall primarily consists of VSMCs and a collagen-rich ECM. VSMCs and fibroblasts produce the ECM, which plays an important role in maintaining the structural integrity of the aortic wall. It has been suggested that TAA pathogenesis is closely correlated with the dysfunction of VSMCs (36). It has also been shown that VSMCs in the aortic wall are a highly dynamic cell population exhibiting continuous phenotypic modulation (37). VSMCs can transform from a differentiated and quiescent contractile state to a proliferative and migratory synthetic phenotype when stimulated, which is characterized by decreased expression of contractile markers and an enhanced rate of VSMC proliferation, migration and synthetic activity (38). In the present study, it was found that Ezh2 knockdown could upregulate contractile marker genes, including *Acta2* and *Tagln*, and downregulate synthetic marker genes, such as *Mmp2* and *Mmp9*. Thus, the results of the present study are consistent with a previous study that showed that deficiency of *Ezh2* allowed for more efficient expression of contractile markers (39,40). Inamoto *et al* (11) reported that the number of contractile aortic SMCs was significantly lower in thoracic aortic tissues with TAD than in healthy aortic tissues, confirming that the transformation of VSMCs from a contractile to a synthetic phenotype may play an important role in TAA. In addition, Ezh2 deficiency effectively reduced the migration potential of VSMCs *in vitro*, which is consistent with the findings previously reported by Han *et al* (12). Taken together, these data indicated that Ezh2 promotes the phenotypic modulation of VSMCs from a synthetic to contractile phenotype, and accelerates the development of TAA (36).

To identify Ezh2 target genes, the effects of Ezh2 on gene expression and pathophysiological signaling pathways were assessed. Several potential candidate genes were identified, as well as pathophysiological pathways targeted by cell adhesion molecule activity and ECM-receptor processes. RNA-seq combined with qChIP experiments revealed that Ezh2 bound directly to the Itgb3 promoter and inhibited Itgb3 expression. This gene is a member of the integrin family, which consists of transmembrane receptors that bridge cell-to-cell and cell-to-ECM interactions, transmitting signals from ECM fibers to the contractile mechanism of VSMCs, allowing VSMCs to initiate transcription in response to these stimuli (13). Integrin activation exerts notable biological roles that regulate ECM assembly, growth factor signaling and cellular functions, such as adhesion, proliferation, survival and migration (41,42) Itgb3, also known as CD61 or GP3A, is one of the most extensively studied ECM family members. ITGB3 plays a key role in determining the proper treatment for tumor, and regulates tumor growth and metastatic spread (41). In addition, ITGB3 plays a pivotal role in promoting and maintaining tumor cell stemness (43). Nevertheless, prior studies have not examined the role of ITGB3 in VSMC proliferation and migration, to the best of our knowledge. The present study showed that *Ezh2* knockdown increased *Itgb3* expression, and *Itgb3* depletion reversed the decrease in SMC migration and calcification

caused by *Ezh2* knockdown, suggesting that ITGB3 may be an inhibitor of EZH2-induced phenotypic transformation of VSMCs in TAA. Taken together, the findings of the present study suggested that the EZH2-ECM-receptor-ITGB3 axis regulates the proliferation and phenotypic switching of VSMCs. Additionally, it was found that Ezh2 transcription inhibited Itgb3 expression; however, further studies are warranted to determine if this is achieved through simultaneous or sequential methylation of H3K27, to broadly maintain an increased level of H3K27me3 at the target promoter, thereby transcriptionally inactivating ECM-receptor genes, such as Itgb3.

In summary, the role of the histone methyltransferase, EZH2, in the phenotypic transformation of SMCs and its involvement in aortic aneurysms was studied. The results showed increased EZH2 levels in human aortic dissection samples and model mice with aortic aneurysms. The enrichment function of EZH2 is focused on ECM processes. RT-qPCR and qChIP experiments confirmed that *Ezh2* inhibited *Itgb3* gene expression by binding to the *Itgb3* gene promoter region, suggesting that the EZH2-ITGB3 regulatory axis is related to smooth muscle phenotypic transformation and the ECM process. The presented findings may aid in the search for therapeutic targets for TAA. EZH2 contributes to the progression of TAA by regulating the phenotypic transformation of VSMCs and the expression of ITGB3. Thus, EZH2 may serve as a suitable target for the management of TAA.

Acknowledgements

The authors would like to thank Dr Ying Li of the Research Center of Translational Medicine, Jinan Central Hospital (Jinan, China) for their assistance in the laboratory.

Funding

This work was supported by grants from the National Natural Science Foundation of China (grant no. 82002987), the China Postdoctoral Science Foundation (grant nos. 2021M691226 and 2022M721334), the Shandong Province Postdoctoral Innovation Talent Support Plan (grant nos. 202102045 and SDCX-ZG-202203007), and the Shandong Medical and Health Science and Technology Development Plan (grant no. 202104020266).

Availability of data and materials

The datasets used and/or analyzed during the current study are available from the corresponding author on reasonable request. The RNA-sequencing dataset generated and/or analyzed during the current study is available in the Gene Expression Omnibus repository (https://www.ncbi.nlm.nih.gov/geo/query/acc.cgi?acc=GSE227177).

Authors' contributions

WY and SX designed the experiments, plotted the graphs and created the diagrams. SX performed the in vitro experiments and was a major contributor in writing the manuscript. FZ and GS collected tissue samples from patients with TAD from Jinan Central Hospital. SX and ZD were responsible for the animal experiments. SX and SL performed the transcriptomics studies. GS and WY confirmed the authenticity of all the raw data. All authors read and approved the final manuscript.

Ethics approval and consent to participate

The studies involving human participants were conducted according to the guidelines of The Declaration of Helsinki, and were reviewed and approved by the Ethics Review Committee of Jinan Central Hospital (approval no. SZR2021-054-01). Informed written consent was obtained from all subjects involved in the study. The animal experiments were approved by the Jinan Central Hospital Experimental Animal Welfare Ethics Review Committee (approval no. JNCHIACUC2022-52).

Patient consent for publication

The patients provided written informed consent for the publication of any data and/or accompanying images.

Competing interests

The authors declare that they have no competing interests.

References

1. Bossone E and Eagle KA: Epidemiology and management of aortic disease: Aortic aneurysms and acute aortic syndromes. Nat Rev Cardiol 18: 331-348, 2021.
2. Bento JR, Meester J, Luyckx I, Peeters S, Verstraeten A and Loeys B: The genetics and typical traits of thoracic aortic aneurysm and dissection. Annu Rev Genomics Hum Genet 23: 223-253, 2022.
3. Lu H, Du W, Ren L, Hamblin MH, Becker RC, Chen YE and Fan Y: Vascular smooth muscle cells in aortic aneurysm: From genetics to mechanisms. J Am Heart Assoc 10: e023601, 2021.
4. Bossone E, LaBounty TM and Eagle KA: Acute aortic syndromes: Diagnosis and management, an update. Eur Heart J 39: 739-749d, 2018.
5. Heiss C, Pitcher A, Belch JJF, De Carlo M, Reinecke H, Baumgartner I, Mazzolai L and Aboyans V: The year in cardiology: Aorta and peripheral circulation. Eur Heart J 41: 501-508b, 2020.
6. Jana S, Hu M, Shen M and Kassiri Z: Extracellular matrix, regional heterogeneity of the aorta, and aortic aneurysm. Exp Mol Med 51: 1-15, 2019.
7. Li C, Qiu S, Liu X, Guo F, Zhai J, Li Z, Deng L, Ge L, Qian H, Yang L and Xu B: Extracellular matrix-derived mechanical force governs breast cancer cell stemness and quiescence transition through integrin-DDR signaling. Signal Transduct Target Ther 8: 247, 2023.
8. Cescon M, Rampazzo E, Bresolin S, Da Ros F, Manfreda L, Cani A, Della Puppa A, Braghetta P, Bonaldo P and Persano L: Collagen VI sustains cell stemness and chemotherapy resistance in glioblastoma. Cell Mol Life Sci 80: 233, 2023.
9. Golledge J: Abdominal aortic aneurysm: Update on pathogenesis and medical treatments. Nat Rev Cardiol 16: 225-242, 2019.
10. Sorokin V, Vickneson K, Kofidis T, Woo CC, Lin XY, Foo R and Shanahan CM: Role of vascular smooth muscle cell plasticity and interactions in vessel wall inflammation. Front Immunol 11: 599415, 2020.
11. Inamoto S, Kwartler CS, Lafont AL, Liang YY, Fadulu VT, Duraisamy S, Willing M, Estrera A, Safi H, Hannibal MC, *et al*: TGFBR2 mutations alter smooth muscle cell phenotype and predispose to thoracic aortic aneurysms and dissections. Cardiovasc Res 88: 520-529, 2010.
12. Han DG, Ahn CB, Lee JH, Hwang Y, Kim JH, Park KY, Lee JW and Son KH: Optimization of electrospun poly(caprolactone) fiber diameter for vascular scaffolds to maximize smooth muscle cell infiltration and phenotype modulation. Polymers (Basel) 11: 643, 2019.

13. Michel JB, Jondeau G and Milewicz DM: From genetics to response to injury: Vascular smooth muscle cells in aneurysms and dissections of the ascending aorta. Cardiovasc Res 114: 578-589, 2018.
14. Aherrahrou R, Baig F, Theofilatos K, Lue D, Beele A, Örd T, Kaikkonen MU, Aherrahrou Z, Cheng Q, Ghosh S, *et al*: Secreted protein profiling of human aortic smooth muscle cells identifies vascular disease associations. medRxiv 10: 23298351, 2023.
15. Zhang L, Xia C, Yang Y, Sun F, Zhang Y, Wang H, Liu R and Yuan M: DNA methylation and histone post-translational modifications in atherosclerosis and a novel perspective for epigenetic therapy. Cell Commun Signal 21: 344, 2023.
16. Ibarrola J, Kim SK, Lu Q, DuPont JJ, Creech A, Sun Z, Hill MA, Jaffe JD and Jaffe IZ: Smooth muscle mineralocorticoid receptor as an epigenetic regulator of vascular ageing. Cardiovasc Res 118: 3386-3400, 2023.
17. Le T, He X, Huang J, Liu S, Bai Y and Wu K: Knockdown of long noncoding RNA GAS5 reduces vascular smooth muscle cell apoptosis by inactivating EZH2-mediated RIG-I signaling pathway in abdominal aortic aneurysm. J Transl Med 19: 466, 2021.
18. Delgado-Olguín P, Dang LT, He D, Thomas S, Chi L, Sukonnik T, Khyzha N, Dobenecker MW, Fish JE and Bruneau BG: Ezh2-mediated repression of a transcriptional pathway upstream of Mmp9 maintains integrity of the developing vasculature. Development 141: 4610-4617, 2014.
19. Wang Y, Huang XX, Leng D, Li JF, Liang Y and Jiang T: Effect of EZH2 on pulmonary artery smooth muscle cell migration in pulmonary hypertension. Mol Med Rep 23: 129, 2021.
20. Li Y, Guo S, Zhao Y, Li R, Li Y, Qiu C, Xiao L and Gong K: EZH2 regulates ANXA6 expression via H3K27me3 and is involved in angiotensin II-induced vascular smooth muscle cell senescence. Oxid Med Cell Longev 2022: 4838760, 2022.
21. Zhuang T, Liu J, Chen X, Pi J, Kuang Y, Wang Y, Tomlinson B, Chan P, Zhang Q, Li Y, *et al*: Cell-specific effects of GATA (GATA Zinc Finger Transcription Factor Family)-6 in vascular smooth muscle and endothelial cells on vascular injury neointimal formation. Arterioscler Thromb Vasc Biol 39: 888-901, 2019.
22. Livak KJ and Schmittgen TD: Analysis of relative gene expression data using real-time quantitative PCR and the 2(-Delta Delta C(T)) method. Methods 25: 402-408, 2001.
23. Ashburner M, Ball CA, Blake JA, Botstein D, Butler H, Cherry JM, Davis AP, Dolinski K, Dwight SS, Eppig JT, *et al*: Gene ontology: Tool for the unification of biology. The Gene Ontology Consortium. Nat Genet 25: 25-29, 2000.
24. The Gene Ontology Consortium: The gene ontology resource: 20 years and still GOing strong. Nucleic Acids Res 47: D330-D338, 2019.
25. Minoru Kanehisa: Post-genome informatics. Oxford University Press, 2000.
26. Wu T, Hu E, Xu S, Chen M, Guo P, Dai Z, Feng T, Zhou L, Tang W, Zhan L, *et al*: clusterProfiler 4.0: A universal enrichment tool for interpreting omics data. Innovation (Camb) 2: 100141, 2021.
27. Pan L, Bai P, Weng X, Liu J, Chen Y, Chen S, Ma X, Hu K, Sun A and Ge J: Legumain is an endogenous modulator of integrin αvβ3 triggering vascular degeneration, dissection, and rupture. Circulation 145: 659-674, 2022.
28. Zhou Y, Wang T, Fan H, Liu S, Teng X, Shao L and Shen Z: Research progress on the pathogenesis of aortic aneurysm and dissection in metabolism. Curr Probl Cardiol 49: 102040, 2023.
29. Chakraborty A, Li Y, Zhang C, Li Y, Rebello KR, Li S, Xu S, Vasquez HG, Zhang L, Luo W, *et al*: Epigenetic induction of smooth muscle cell phenotypic alterations in aortic aneurysms and dissections. Circulation 148: 959-977, 2023.
30. Pinard A, Jones GT and Milewicz DM: Genetics of thoracic and abdominal aortic diseases. Circ Res 124: 588-606, 2019.
31. Chang CJ and Hung MC: The role of EZH2 in tumour progression. Br J Cancer 106: 243-247, 2012.
32. Rao ZY, Cai MY, Yang GF, He LR, Mai SJ, Hua WF, Liao YJ, Deng HX, Chen YC, Guan XY, *et al*: EZH2 supports ovarian carcinoma cell invasion and/or metastasis via regulation of TGF-beta1 and is a predictor of outcome in ovarian carcinoma patients. Carcinogenesis 31: 1576-1583, 2010.
33. Mitić T, Caporali A, Floris I, Meloni M, Marchetti M, Urrutia R, Angelini GD and Emanueli C: EZH2 modulates angiogenesis in vitro and in a mouse model of limb ischemia. Mol Ther 23: 32-42, 2015.
34. Liu Y, Dai C, Lei Y, Wu W and Liu W: Inhibition of EZH2 attenuates coronary heart disease by interacting with microRNA-22 to regulate the TXNIP/nuclear factor-κB pathway. Exp Physiol 105: 2038-2050, 2020.
35. Aljubran SA, Cox R Jr, Parthasarathy PT, Ramanathan GK, Rajanbabu V, Bao H, Mohapatra SS, Lockey R and Kolliputi N: Enhancer of zeste homolog 2 induces pulmonary artery smooth muscle cell proliferation. PLoS One 7: e37712, 2012.
36. Yuan Y, Wang C, Xu J, Tao J, Xu Z and Huang S: BRG1 overexpression in smooth muscle cells promotes the development of thoracic aortic dissection. BMC Cardiovasc Disord 14: 144, 2014.
37. He D, Mao A, Zheng CB, Kan H, Zhang K, Zhang Z, Feng L and Ma X: Aortic heterogeneity across segments and under high fat/salt/glucose conditions at the single-cell level. Natl Sci Rev 7: 881-896, 2020.
38. Owens GK, Kumar MS and Wamhoff BR: Molecular regulation of vascular smooth muscle cell differentiation in development and disease. Physiol Rev 84: 767-801, 2004.
39. Cardenas CL, Kessinger CW, MacDonald C, Jassar AS, Isselbacher EM, Jaffer FA and Lindsay ME: Inhibition of the methyltranferase EZH2 improves aortic performance in experimental thoracic aortic aneurysm. JCI insight 3: e97493, 2018.
40. McDonald RA, Hata A, MacLean MR, Morrell NW and Baker AH: MicroRNA and vascular remodelling in acute vascular injury and pulmonary vascular remodelling. Cardiovasc Res 93: 594-604, 2012.
41. Zhu C, Kong Z, Wang B, Cheng W, Wu A and Meng X: ITGB3/CD61: A hub modulator and target in the tumor microenvironment. Am J Transl Res 11: 7195-7208, 2019.
42. Yang X, Xu C, Yao F, Ding Q, Liu H, Luo C, Wang D, Huang J, Li Z, Shen Y, *et al*: Targeting endothelial tight junctions to predict and protect thoracic aortic aneurysm and dissection. Eur Heart J 44: 1248-1261, 2023.
43. Desgrosellier JS and Cheresh DA: Integrins in cancer: Biological implications and therapeutic opportunities. Nat Rev Cancer 10: 9-22, 2010.